

Indirect measurements of the mass balance of summer Arctic sea ice with an electromagnetic induction technique

H. EICKEN,¹ W. B. TUCKER, III,² D. K. PEROVICH²

¹*Geophysical Institute, University of Alaska Fairbanks, Fairbanks, AK 99775-7320, U.S.A.*

²*Cold Regions Research and Engineering Laboratory, U.S. Army Corps of Engineers, 72 Lyme Road, Hanover, NH 03775-1290, U.S.A.*

ABSTRACT. In the framework of the Surface Heat Budget of the Arctic (SHEBA) study, indirect, non-invasive ice mass-balance measurements were carried out at a drifting station in the northern Chukchi Sea between May and August 1998. Ice thickness was derived from electromagnetic induction (EM) measurements of apparent conductivity along 13 profiles (60–900 m long). As shown through sensitivity studies with a one-dimensional model, the apparent conductivity data from individual points can be inverted to yield estimates of ice thickness and ablation with an accuracy of approximately 0.05 m (for 2 m thick level ice). Ablation rates were 8–18 mm d⁻¹, with total ablation amounting to roughly 0.9–1.2 m. Measurements of thickness and melt rates along different profiles in undeformed multi-year ice corresponded closely, indicating that the sampling statistics are adequate. The roughness of undeformed ice has been found to increase during the summer due to deepening of melt ponds and enhanced bottom melt. Ice under melt ponds was disproportionately thinner, most likely a result of thicker snow cover reducing winter accretion.

1. INTRODUCTION

Undeformed sea ice in the Arctic basin typically experiences 0.1–1 m of surface and bottom melt during the summer period (Maykut, 1986; Romanov, 1996). The magnitude as well as the spatial and temporal variability of summer ablation are of great importance in determining the overall mass balance of the Arctic ice pack. Satellite and ground-based observations indicate that extent and thickness of the Arctic sea-ice cover have undergone significant changes in recent decades (Cavalieri and others, 1997; Rothrock and others, 1999), although it is not clear to what extent these are the result of natural variability. Nevertheless, it is apparent that a significant fraction of these changes have been confined to the ablation season (Maslanik and others, 1996; Perovich and others, 1999b; Haas and Eicken, 2001), underscoring the importance of summer melt processes in determining the state of the Arctic ice pack.

Measurements of annual loss and gain of ice mass are required at selected sites to improve our understanding of the ice-growth and ablation processes and to enhance their representation in numerical sea-ice models. As part of the Surface Heat Budget of the Arctic Ocean (SHEBA) project, ice mass-balance data were collected at a drifting station in the northern Chukchi Sea and Beaufort Sea from October 1997 to October 1998 (Perovich and others, 1999b). Traditionally, such mass-balance data are collected by repeated thickness-gauge measurements, with a crossbar on a wire pulled up against the ice bottom and read against a scale on a gauge anchored into the ice. While this robust and time-proven method has distinct advantages, even with a large effort it only provides spot measurements at a restricted number of points. During the ablation period when changes in ice thickness are most rapid, absorption of shortwave radiation can cause

problems with loosening and enhanced formation of puddles around gauges. At a later stage, the hydraulic conduit provided by the wire and gauge leads to drainage of meltwater, potentially affecting the small-scale energy and mass balance.

During summer 1998 an electromagnetic induction (EM) method was tested and validated at the SHEBA site as an alternative approach to mass-balance measurements. The EM method relies on the strong conductivity contrast between the ice cover and the underlying sea water, registering the strength of a secondary magnetic field below the ice bottom that is induced by the primary field generated by the instrument. While the method is not as accurate (in particular on shorter time-scales), it has two distinct advantages over conventional thickness-gauge measurements: it provides larger datasets in a shorter period of time and is non-destructive, thereby minimizing problems due to shortwave absorption by gauge installations in summer. EM techniques have been successfully employed to obtain thickness data in different regions, mostly during the cold winter months when ice conductivities are at their minimum (Kovacs and others, 1987; Multala and others, 1996; Haas and others, 1997). The aim of this investigation is to (1) assess the sensitivity and accuracy of EM methods for ablation measurements, (2) derive an ice conductivity–thickness relationship to allow for inversion of apparent-conductivity measurements at the SHEBA site, (3) determine the contribution and spatial variability of ablation to the mass balance of the ice cover based on the EM datasets, and (4) examine ablation data collected along a profile in ponded ice.

2. STUDY AREA AND OVERVIEW OF MEASUREMENT PROGRAM

During May–August 1998, Ice Station SHEBA drifted

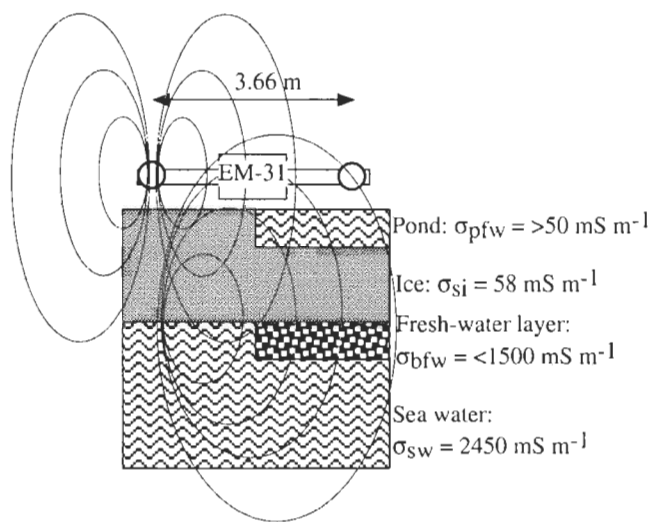


Fig. 1. Schematic depiction of EM device with transmitter and receiver coils, primary/secondary field and the position and conductivity of different layers discussed further in the text.

between 76° and 78.5° N and 160° and 170° E in the northern Chukchi Sea (Perovich and others, 1999b). The core component of the SHEBA site extended over an area of approximately 10 km^2 , composed of a mixture of first- and multi-year ice, the former mostly in the form of refrozen leads. A total of 135 thickness gauges were distributed among 10 sites (for details of site layout and further information on measurement program see Perovich and others, 1999a). Gauges were read at intervals of 2–4 days during the summer period. EM thickness data were obtained along 13 profiles at 7 of the main mass-balance sites, varying between 60 and 900 m in length with measurements at intervals of 2.5 (topographic profiles 1 and 2) to 5 m.

EM measurements were carried out with a Geonics EM-31 device. The instrument determines the apparent conductivity of the underlying medium based on measurements of the secondary electromagnetic field that a surface-based transmitter coil induces in the ice and the sea water underneath (Fig. 1). Owing to low bulk sea-ice conductivities ($< 80 \text{ mS m}^{-1}$) and high sea-water conductivities ($> 2400 \text{ mS m}^{-1}$), the signal is controlled by eddy currents generated at the ice–sea-water interface. The two coplanar transmitter and receiver antenna coils are mounted at a spacing of 3.66 m and operate at 9.8 kHz. The entire instrument has been mounted in a polyethylene kayak hull to place it as close to the surface as possible and increase the ease of towing by hand and snowmobile across the ice and melt ponds. All measurements reported here were carried out in the horizontal dipole mode, yielding a footprint that is approximately 1.35 times larger than the distance between the instrument and the ice/water interface (Liu and Becker, 1990). During the early season, the co-location error between the same point at different dates is $< 5 \text{ m}$ for the profile along the main line (including Ridge and Pittsburgh; see Perovich, 1999a, for locations) and $< 2 \text{ m}$ for Seattle, Sarah's Lake and surface topography profiles. Along the 900 m long profile beyond Tuk and at Atlanta the maximum offset between profiles is estimated as 10 m. Later in the season, positioning errors increase along the main line and beyond Tuk due to floe break-up and extensive melt.

In addition to these measurements, the surface topography of the ice was determined with a laser levelling device at 0.5–1 m spacing. Ice-salinity data were obtained with a

YSI 30 conductivity sonde on melted ice cores that had been cut into 0.05–0.1 m segments immediately after sampling. Ice temperatures were measured by inserting a temperature probe into small holes drilled into the ice core.

3. VALIDATION OF ICE-THICKNESS/APARENT-CONDUCTIVITY RELATIONSHIPS

The EM measurements yield an apparent conductivity σ_a that is derived from the ratio of the imaginary components of the primary and secondary field H_p and H_s according to

$$\sigma_a = \frac{2}{\pi f \mu_0 r^2} \text{Im} \left\{ \frac{H_s}{H_p} \right\} \quad (1)$$

with the magnetic permeability of free space $\mu_0 = 4\pi \times 10^{-7} \text{ H m}^{-1}$, a coil separation r of 3.66 m and at a frequency f of 9.8 kHz. The apparent conductivity depends on the conductivity structure of the half-space below the instrument and is dominated by the sea-water component. The mean salinity of the water column at 4–10 m depth, i.e. directly underlying the ice, has been determined as $30.7 \pm 0.4 \text{ psu}$ (practical salinity units) for the period 1 June–31 August 1998, based on the dataset compiled by T. Stanton and others (available through the Joint Office for Science Support (JOSS) CODIAC data distribution system). At a mean temperature of -1.65°C this corresponds to a conductivity of approximately 2450 mS m^{-1} . The sea-ice conductivity has been derived from profile measurements of ice salinity and temperature at three of the mass-balance sites. Given the brine-volume fraction V_b (computed according to Cox and Weeks, 1983) and the brine conductivity σ_b according to Stogryn and Desargant (1985), the bulk ice conductivity σ_i has been determined according to Archie's law

$$\sigma_i = \sigma_b V_b^m \quad (2)$$

with the exponent set to $m = 1.75$ as outlined in Haas and others (1997). This yields an average ice conductivity of 58 mS m^{-1} , with σ_i varying between 42 and 70 mS m^{-1} .

With most of the ablation measurements carried out in comparatively level sea ice of thicknesses $z_i \leq 4 \text{ m}$, one-dimensional modeling of the apparent-conductivity signal provides a basis for inversion of the conductivity datasets. The relative magnitude of H_s is derived as a function of the height above layers of varying thickness and conductivity as outlined in Haas and others (1997) and following Ward and Hohmann (1988). Figure 2 shows the model results based on the ice and sea-water conductivities described above and for varying ice thickness. For comparison, 66 EM measurements directly adjacent to thickness gauges have also been plotted and agree very well with the model. Discrepancies are in large part attributed to potential offset between the gauge and the instrument as well as the different footprint sizes for the gauge ($< 0.2 \text{ m}$) and the EM-31 ($> 2 \text{ m}$). The one-dimensional model curve has been approximated by an exponential function

$$\sigma_i = 57.34 + 958.1 \exp(-0.8406 z_i) \quad (R^2 > 0.999) \quad (3)$$

which yields the transformation equation to derive ice thickness from conductivity measurements as

$$z_i = 8.167 - \frac{\ln(\sigma_i - 57.35)}{0.8406} \quad (4)$$

Also shown in Figure 2 is an empirical relationship derived

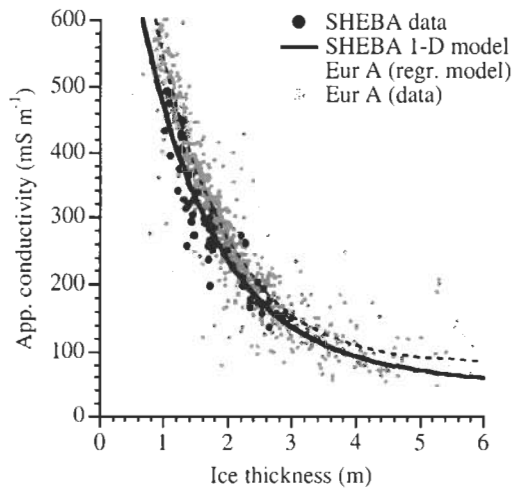


Fig. 2. Ice-thickness/conductivity relationship for EM measurements at SHEBA thickness gauges. The solid line is derived from a one-dimensional model based on mean ice and water conductivities during summer. The dashed line corresponds to an empirical relationship (Equation (5)) derived for a larger dataset of measurements (grey symbols) in the Eurasian Arctic (Haas and Eicken, 2001).

for comparable summer sea ice in the Eurasian Arctic (Haas and Eicken, 2001)

$$\sigma_i = 79.5 + 1139.8 \exp(-0.913z_i), \quad (5)$$

which integrates a larger component of thicker, deformed ice but appears to overestimate thickness based on the SHEBA data. This may in part be due to the lower surface sea-water conductivities observed at the SHEBA site. In this study, all derived ice thicknesses are based on Equation (4), with a comparative analysis of data transformed with the inverted Equation (5).

4. SENSITIVITY TO VARIATIONS IN THE CONDUCTIVITY STRUCTURE OF ARCTIC SUMMER SEA ICE AND ACCURACY OF THE METHOD

Despite the high volume fractions of brine or meltwater in summer sea ice (exceeding 10% in many layers), the overall ice conductivity is still comparatively low, with an average value of $< 60 \text{ mS m}^{-1}$, due to the low salinity of the partially snow-derived meltwater. This circumstance accounts for the superiority of EM vs active radar-frequency techniques in the study of ice thickness in summer. Nevertheless, the presence of meltwater layers at the surface in the form of ponds and directly underneath the ice does affect the EM signal. To assess the sensitivity of the method to layers of different thickness and salinity, the effective deviation from the true ice thickness as measured by the EM-31 in the present configuration has been derived with the one-dimensional model (see Fig. 1 for different layer configurations). As shown in Figure 3, ice thickness is underestimated by approximately 0.1 m for a pond of salinity 10‰ and 0.08 m depth or of salinity 2.5‰ and 0.28 m depth. Due to low average pond salinities of 0.3‰, the deviations are on the order of 0.01 m for most of the melt season (largely independent of pond thickness as evident from Fig. 3), which is also supported by direct thickness measurements in ponded areas. In the last weeks of August, with average salinity increasing to 7‰, deviations as high as 0.5 m can result for a pond depth of around 0.4 m.

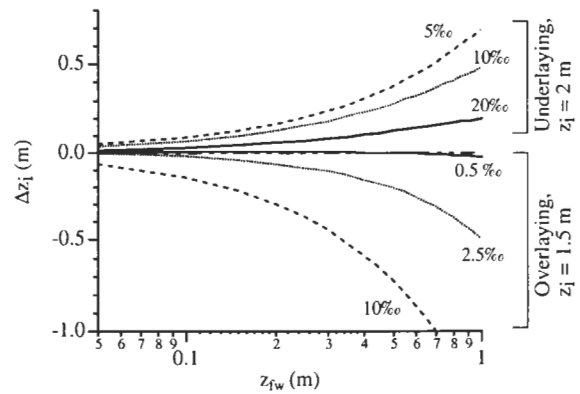


Fig. 3. Deviations Δz_i of measured from true ice thickness z_i as derived from one-dimensional EM modeling for a layer of fresh or brackish water of thickness z_{fw} underlying or overlying an ice cover of 2 m (overlying) or 1.5 m (underlying) thickness. The salinity of the water layer is indicated at right; the dashed-dotted line corresponds to $\Delta z_i = 0$.

Thus, in the presence of saline melt ponds, their impact on the signal must be corrected for.

Under-ice water layers of low salinity ($< 10\text{‰}$) result in an apparent increase in ice thickness by $> 0.1 \text{ m}$ for layer thicknesses above 0.2 m. Higher-salinity ($> 20\text{‰}$) layers require thicknesses in excess of 0.4 m for the same effect. Since formation of fresh under-ice water lenses is not uncommon in the Arctic (Eicken, 1994), it is advisable to check for their presence. At SHEBA, under-ice ponds were observed under first-year ice and in thinner sections of multi-year floes, with layer thicknesses of 0.1–0.5 m and salinities of $< 5\text{‰}$, resulting in overestimates of ice thickness by 0.05–0.3 m. Except for parts of the 900 m profile beyond Tuk, they did not appear to significantly affect the mass-balance gauge sites and conductivity data, however, and have hence not been corrected for. Given the spatial heterogeneity of such under-ice melt lenses, correction for these effects is possible but may require more intensive EM/drill-data comparisons or surveys of the under-ice salinity structure. In most cases, the impact of such lenses on the accuracy of the data is deemed tolerable, however.

The accuracy of the EM31 instrument is specified at better than 1 mS m^{-1} . Based on the first derivative of the empirical thickness–conductivity relations, this translates to a sensitivity of 0.015 m for 3 m thick level ice and 0.09 m for 5 m thick level ice. Uncertainties in the distance between the instrument and the ice surface and in coil orientation increase the total measurement error to approximately 0.05 m for 2 m thick ice when compared against drillhole or gauge ice-thickness measurements. Because of the different footprint size of EM vs drillhole or gauge measurements ($> 2 \text{ m}$ vs $< 0.2 \text{ m}$), a significant fraction of the disparities (as well as the scatter evident in Fig. 2) result from the mismatch in sampled ice surface area rather than from true discrepancies. Taking into account such errors associated with drillhole or gauge measurements and averaging over repeat profile measurements results in an error estimated at approximately 0.05 m (level ice thickness 2 m) for the present dataset. As derivation of ice thicknesses in ridged ice sections with keel depths larger than approximately 7.5 m or level ice thicknesses $> 6 \text{ m}$ requires two-dimensional modelling and further data analysis, ablation measurements have been restricted to ice thicknesses smaller than these critical thresholds.

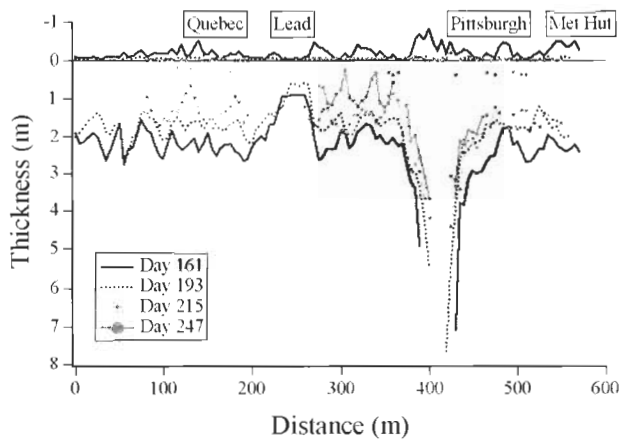


Fig. 4. EM measurements of ice thickness (5m spacing) along the main ablation line (including Pittsburgh and Ridge sites) during the course of the ablation season. Note that thickness axis has been reversed so as to roughly match floe bottom topography. Snow (completely gone by day 193) or melt-pond depths (individual points visible below zero line) are plotted at the top, drawn to scale but with reversed sign compared to thickness data. Data missing along the profile later in the season are result of floe disintegration.

5. MASS-BALANCE MEASUREMENTS AT THE SHEBA FIELD SITE

The impact of the ablation season on a large segment of the SHEBA camp floe is evident from Figure 4, which shows the EM-derived thickness profile along a 600m section that encompasses the main ablation line as well as the Quebec, Pittsburgh and Ridge sites. The bottom of the ridge extended to depths to render interpretation of conductivity measurements based on a one-dimensional approach unreliable. The highest melt rates were observed on the flank of the ridge towards the Met Hut, with a total ablation of up to 1.5m between days 161 and 247. While smaller topographic features are difficult to match directly in different profiles, an increase in ice roughness, due mostly to deepening puddles (e.g. 290–370 m), is evident in parts of the profile. Thinning of lead ice is also pronounced, with disintegration of the floe along the Quebec lead later in the ablation period. While a more detailed study of the evolution of ice roughness is beyond the scope of this paper, it is noteworthy that the standard deviation of ice thickness (as a simple roughness measure) is increasing during the ablation season in both relative and absolute terms for all profiles except the main line, where disintegration of the ice towards the end of the season limits an assessment of roughness (Table 1; see also section 6).

The impact of the ablation season on the ice-thickness distribution as derived from the combined dataset is shown in Figure 5. The mode of the distribution has been shifted by approximately 1.2 m. The widening of the distribution is only in part due to actual differences in ablation rates for different thickness classes. A limited subset of gauge data (Fig. 6b) indicates little dependence of ablation on initial ice thickness, but such dependence is more pronounced for the entire dataset. The broadening in distribution is also a result of temporal differences in the acquisition of the datasets during the last part of the ablation season (Table 1). Given that co-location errors are comparatively small, spatial variability is not deemed to be of significance here.

Table 1. Ice thickness z_i (mean and standard deviation) at day of year D , total amount of ice ablation Δz_{tot} and ablation rates $\Delta z/\Delta t$ at different sites

Location	$z_{i,0}$ m	D_0	$z_{i,1}$ m	D_1	Δz_{tot} m	$\Delta z/\Delta t$ mm d ⁻¹
Atlanta	1.81 ± 0.31	154	1.35 ± 0.40	209	0.46	-8
Seattle	2.64 ± 0.50	162	1.68 ± 0.52	215	0.96	-18
Main line	2.74 ± 1.12	161	1.49 ± 0.90	247	1.25	-14
Tuk	1.78 ± 0.49	154	0.88 ± 0.55	243	0.90	-10
Topol	1.69 ± 0.24	173	0.81 ± 0.32	239	0.88	13

* Only data points representing ice present at start and end of season have been taken into account.

The magnitude and rate of ablation at the individual main sites are listed in Table 1. The actual length of the ice ablation season (based on the period between the onset and termination of ice, rather than snowmelt) depends on several factors, including the depth of the snow cover and the ice thickness. Generally, surface ice melt commenced between 16 and 22 June (days 167 and 173) after removal of the snow cover and ended in mid- to late August (day 230 and later). Bottom melt started around 2 June (day 153) and ended by late September (day 270 or later). Snowmelt commenced on 29 May (day 149). Thus, the longest records (main line, topography profile 1 and Tuk) cover almost the entire surface ablation season and most of the bottom ablation period. The total amount of ablation between these three sites agrees to within 20%, with maximum ablation rates observed in the thicker, ridged sections.

Ablation rates at Atlanta and Seattle are more difficult to interpret due to the shorter measurement interval. With a general increase in the ablation rates during stages two and three of the season (Fig. 6), Atlanta does appear to be in the same range as the other locations if measurements had been continued over a longer interval. The three stages of the melt season shown in Figure 6a have been defined by (1) snowmelt and subsequent drainage of ponds, (2) expansion of ponds due to lateral melting, and (3) disintegration of the ice cover in the aftermath of a storm (for a more detailed

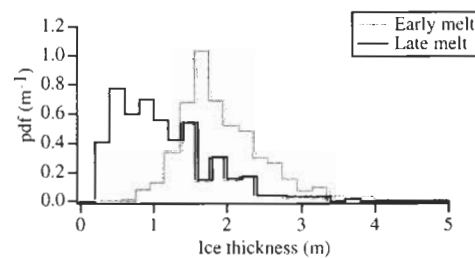


Fig. 5. Probability density function (pdf) of ice thickness for entire EM-derived dataset in the early and late melt season (413 and 390 measurements, respectively). Measurement time intervals are: days 154–209 (Atlanta), 162–215 (Seattle), 161–247 (main line), 173–239 (Topol), 154–209 (Tuk), with each first day corresponding to the “early melt” and each second day to the “late melt” curve.

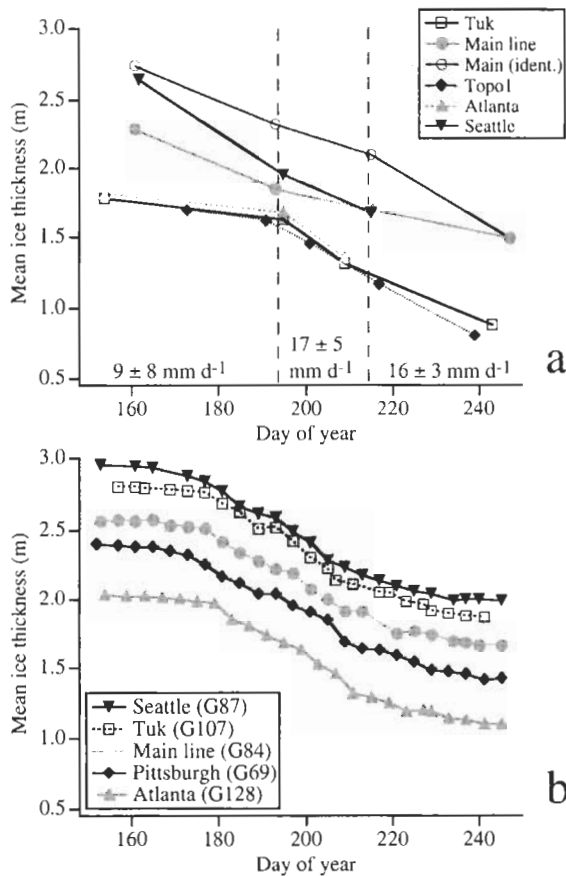


Fig. 6. (a) Changes in mean EM-derived ice thickness for five major ablation measurement sites or profiles during the course of the melt season. Open circles for main ablation line are for contiguous data points at positions throughout the melt season (see Fig. 4). Numbers indicate the average daily ablation rates for three major time intervals (dashed lines). (b) Changes in ice thickness at single gauges during the same time period (gauge numbers are in parentheses).

discussion of the temporal ice evolution during the melt season see Eicken and others, in press). The thinning rates at Seattle are higher most likely because measurements have been carried out along a series of profiles perpendicular to the adjacent lead, with the heat flux from the water to the bottom of the ice significantly enhanced by solar heating of the lead at this site. However, there was no steady gradient in ablation rate discernible perpendicular to the lead.

The seasonal evolution of ice ablation, at least as far as it is evident from this limited number of measurements, is summarized in Figure 6. At most sites, melt accelerated into the latter part of the ablation season. This could be the result of enhanced turbulent transfer of heat stored in leads and melt ponds to the ice bottom in the aftermaths of increased synoptic meteorological activity and break-up of the SHEBA ice floe (Richter-Menge and Perovich, 2001; Eicken and others, in press). In general, however, the agreement between indirect, EM thickness measurement and those of a selection of gauges at the same sites correspond quite well as shown in Figure 6b.

A striking feature evident in Figure 6a is the close correspondence in overall ice thickness and ablation rates between the three profiles located in mostly undeformed multi-year ice at the main camp (topography profile 1, Atlanta and Tuk (100, 220 and 900 m long, respectively; no significant differences at the $p = 0.95$ level for all datasets). This good agree-

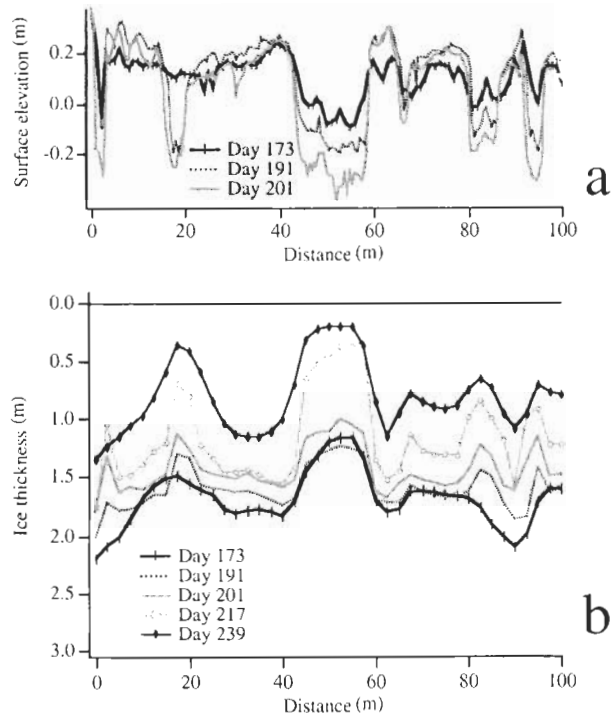


Fig. 7. Surface elevation (a), measured at 0.5–1 m intervals, and ice-thickness profile (b), measured at 2.5 m intervals, along topography profile 1. Note that ice-thickness axis has been reversed so as to roughly match floe bottom topography.

ment suggests that for undeformed second- or multi-year sea ice, the EM thickness (or ablation) data are representative samples of the respective ice-thickness class. Given that the different profiles are spaced up to several km apart, i.e. at a separation ensuring statistically independent samples based on typical autocorrelation lengths for Arctic sea ice, this is actually quite encouraging, in particular with respect to parameterization and modelling of level-ice ablation.

6. ABLATION MEASUREMENTS ALONG A PROFILE OF UNDEFORMED, POND-COVERED SEA ICE

As pointed out above, EM techniques are particularly suited for mass-balance measurements because they are non-invasive and allow for acquisition of data points along profiles. These strengths are important for measurements in summer sea ice covered with melt ponds, as the latter have a pronounced effect on the local mass balance and may furthermore be adversely impacted by direct thickness measurements, prone to enhance pond drainage. At the SHEBA site, the thickness evolution of a section of undeformed, ponded multi-year ice (topography profile 1, 100 m long) was monitored during the course of the melt season, with average ice thickness decreasing from 1.69 to 0.81 m (Fig. 7; Table 1). In agreement with the general trend, deepening of ponds (Fig. 7a), and to a lesser extent enhanced bottom melt underneath ponds, contributes substantially to an overall increase in the roughness of undeformed ice during the summer. This is exemplified by an increase in the standard deviation of ice thickness along the profile by one-third during the summer (Table 1). At the lower ice surface, the spatial resolution of EM measurements does not allow quantitative conclusions about small-scale roughness, but roughening of the upper surface is clearly expressed

with a 2.5-fold increase in standard deviation σ_{se} of ice surface elevation from 0.08 to 0.20 m along the Topol profile (Fig. 7a; even if only the bare-ice and pond-water surface are taken into account, σ_{se} still increases by almost a third).

The EM thickness measurements along the profile are only marginally affected by the pond fresh-water layer. Through day 201, pond salinities did not exceed 0.3‰, with average pond depths of 0.08–0.26 m. Infiltration of brine and sea water during the last part of the melt season resulted in an increase of pond salinity to 0.8–1.1‰ at depths of 0.22–0.36 m (i.e. salinities significantly lower than the mean pond salinity which amounted to roughly 7‰ in early August). Based on the one-dimensional model results presented in section 4 (Fig. 3), this would result in an underestimate of ice thickness by at most 0.06 m.

The enhanced melt rates of ice beneath melt ponds, both at the surface and from below, evident also in the profile shown in Figure 7, have been discussed in the context of enhanced absorption of solar shortwave radiation (see Eicken, 1994). Linkages between melt ponds and large-scale depressions in the ice bottom due to this phenomenon have been considered as prerequisites for the formation of under-ice melt ponds, characterized by summer ice growth at the interface between a fresh-water lens trapped underneath a pond and overlying cold sea water (Wadhams and Martin, 1990; Eicken, 1994). The ice underlying the large pond 40–60 m along the profile shown in Figure 7 (and to some extent also the one at approximately 20 m) was already substantially thinner than the surrounding portions even before the removal of a snow cover and the establishment of open melt ponds. This was also observed along the profiles at Atlanta and Tuk. Evidence from ice coring and field observations suggests that the position of these ponds in many cases corresponded to the locations of ponds in the previous melt season. Hence, a disproportionately deep snow cover over former melt ponds, with snow being trapped in the topographic lows, might in part be responsible for reduced ice-growth rates due to enhanced thermal insulation from the atmosphere (Perovich and Elder, 2001). This would explain the presence of thinner ice under melt ponds at the start of the melt season and might even be a recurring process amplified over the course of several summers for older ice as indicated by SHEBA ice-floe temperature profile data (Perovich and Elder, 2001). While further investigations are required to substantiate this hypothesis, it appears that EM measurements hold considerable promise for the investigation of such processes.

7. SUMMARY AND CONCLUSIONS

An extensive set of indirect ice-thickness measurements carried out with an EM device at the SHEBA site during summer 1998 demonstrated that the EM method is well suited to the task of obtaining mass-balance data for mostly undeformed ice < 5 m thick. The success of the method is in large part dependent on low sea-ice conductivities, determined as < 60 mS m⁻¹, and low to moderate surface melt pond conductivities (mostly < 100 mS m⁻¹). With an accuracy of approximately 0.05 m for a total ablation of roughly 0.9–1.2 m at the SHEBA site, EM measurements are valuable both for stand-alone acquisition of mass-balance datasets (preferably including additional direct ice-thickness determinations to help constrain thickness-conductivity

models) and as a supplementary technique that helps integrate point-type mass-balance data into a large-scale context. The good agreement between the individual EM datasets and their close correspondence to thickness-gauge data indicate a sufficiently high sampling density for the SHEBA mass-balance program.

Seasonal variability of EM-derived ablation rates at the SHEBA site roughly conforms with three stages of the summer melt seasons, established on the basis of key melt events (disappearance of snow and drainage of melt ponds; expansion of ponds due to lateral melting; ice break-up and disintegration; see Eicken and others, in press, for details). Ablation rates are generally higher during the last two stages of melt, most likely as a result of decreases in ice albedo and increases in turbulent heat transfer at both the air/ice and the ice/water interface. Since the freeze-up process which extends well into October (Perovich and others, 1999b) has not been captured in this study, there is no evidence of melt deceleration at the close of the season. These temporal patterns are evident in individual thickness-gauge records of higher temporal resolution as well.

The EM data also show differences in ablation rates for ice of different thickness categories, evident both in the overall probability density function of the dataset as well as in individual profiles. In part, these differences are attributed to temporal differences in the sampling intervals. Evidence from the entire dataset and from individual gauges suggests that such thickness-ablation dependence is not as pronounced for level multi-year ice, but strongly affects ridges and thinner ice. Of particular interest are repeated thickness and surface elevation measurements along a profile through undeformed sea ice that provide insight into the development and evolution of melt features such as melt puddles and bottom depressions. The latter appear to be associated with surface melt ponds, most likely as a result of reduced ice-growth rates under a thicker, thermally insulating snow cover. At the same time, high-resolution surface topography and overall thickness data indicate an increase in small-scale ice roughness during the ablation season, mostly as a result of deepening of ponds. The non-invasive nature of the EM method and its reliability in the measurement of undeformed ice of intermediate thickness predestine the technique both for routine mass-balance measurements and for process studies of the evolution of ice-floe top and bottom topography.

ACKNOWLEDGEMENTS

Support by the U.S. National Science Foundation grant OPP-9872626 and Office of Naval Research Grant N00014-97-1-0765 is gratefully acknowledged. Thanks go to the CCG *Des Groseilliers* and the SHEBA Project Office teams for their support both on and off the ship. Numerous people helped with different aspects of the fieldwork; their support is much appreciated. Comments by M. Lange and an anonymous reviewer helped to improve the manuscript.

REFERENCES

- Cavalieri, D. J., P. Gloersen, C. L. Parkinson, J. C. Comiso and H. J. Zwally. 1997. Observed hemispheric asymmetry in global sea ice changes. *Science*, **278**(5340), 1104–1106.
- Cox, G. F. N. and W. F. Weeks. 1983. Equations for determining the gas and brine volumes in sea-ice samples. *J. Glaciol.*, **29**(102), 306–316.

- Eicken, H. 1991. Structure of under-ice melt ponds in the central Arctic and their effect on the sea-ice cover. *Limnol. Oceanogr.*, **39**(3), 682–694.
- Eicken, H., H. R. Krouse, D. Kadko and D. K. Perovich. In press. Tracer studies of pathways and rates of meltwater transport through Arctic summer sea ice. *J. Geophys. Res.*
- Haas, C. and H. Eicken. 2001. The thickness distribution of summer sea ice in the Laptev Sea and the adjacent sector of the Arctic Ocean. *J. Geophys. Res.*, **106**(C3), 4419–4462.
- Haas, C., S. Gerland, H. Eicken and H. Miller. 1997. Comparison of sea-ice thickness measurements under summer and winter conditions in the Arctic using a small electromagnetic induction device. *Geophysics*, **62**(3), 749–757.
- Kovacs, A., N. D. Valleau and J. S. Holladay. 1987. Airborne electromagnetic sounding of sea ice thickness and sub-ice bathymetry. *Cold Reg. Sci. Technol.*, **14**(3), 289–311.
- Liu, G. and A. Becker. 1990. Two-dimensional mapping of sea-ice keels with airborne electromagnetics. *Geophysics*, **55**(2), 239–248.
- Maslanik, J. A., M. C. Serreze and R. G. Barry. 1996. Recent decreases in Arctic summer ice cover and linkages to atmospheric circulation anomalies. *Geophys. Res. Lett.*, **23**(13), 1677–1680.
- Maykut, G. A. 1986. The surface heat and mass balance. In Untersteiner, N., ed. *Geophysics of sea ice*. London, etc., Plenum Press, 395–463. (NATO ASI Series B: Physics 146.)
- Multala, J. and 7 others. 1996. An airborne electromagnetic system on a fixed wing aircraft for sea ice thickness mapping. *Cold Reg. Sci. Technol.*, **24**(4), 355–373.
- Perovich, D. K. and B. C. Elder. 2001. Temporal evolution of Arctic sea-ice temperature. *Ann. Glaciol.*, **33** (see paper in this volume).
- Perovich, D. K. and 8 others. 1999a. *SHEBA: snow and ice studies*. Hanover, NH, U.S. Army Corps of Engineers, Cold Regions Research and Engineering Laboratory.
- Perovich, D. K. and 22 others. 1999b. Year on ice gives climate insights. *EOS*, **80**(41), 481, 485–486.
- Richter-Menge, J. A., D. K. Perovich and S. Pegau. 2001. Summer ice dynamics during SHEBA and its effect on the ocean surface heat content. *Ann. Glaciol.*, **33** (see paper in this volume).
- Romanov, I. P. 1996. *Atlas of ice and snow of the Arctic Basin and Siberian Shelf seas. Second edition*. Fair Lawn, NJ, Backbone Publishing Company.
- Rothrock, D. A., Y. Yu and G. A. Maykut. 1999. Thinning of the Arctic sea-ice cover. *Geophys. Res. Lett.*, **26**(23), 3469–3472.
- Stogryn, A. and G. J. Desargant. 1985. The dielectric properties of brine in sea ice at microwave frequencies. *IEEE Trans. Antennas Propag.*, **AP-33**(5), 523–532.
- Wadhams, P. and S. Martin. 1990. Processes determining the bottom topography of multiyear arctic sea ice. *CRREL Monogr.* 90-1, 136–141.
- Ward, S. H. and G. W. Hohmann. 1988. Electromagnetic theory for geophysical applications. In Nabighian, M. N., ed. *Electromagnetic methods in applied geophysics — theory. Vol. 1*. Tulsa, OK, Society of Exploration Geophysicists, 131–313. (Monograph 3.)